Assessment of variability of TEC and improvement of performance of the IRI model over Ethiopia during the high solar activity phase

Yekoye Asmare Tariku

Department of Space Science and Research Application Development, Ethiopian Space Science and Technology Institute, Addis Ababa, Ethiopia

* Corresponding author. Tel. +251912799754

Email_address:yekoye2002@gmail.com (Yekoye Asmare)

Abstract

This paper discusses the monthly and seasonal variation of the total electron content (TEC) and the improvement of performance of the IRI model in estimating TEC over Ethiopia during the solar maximum (2013-2016) phase employing GPS TEC data inferred from the GPS receivers installed at different regions of Ethiopia. **The results reveal that, in the year 2013-2016, the highest peak measured seasonal diurnal VTEC value is observed in the March equinox in 2015 over Arba Minch station**. Moreover, both the arithmetic mean measured and modeled VTEC values, generally, show maximum and minimum values in the equinoctial and June solstice months, respectively in 2014-2015. **However, in 2013, the minimum and maximum arithmetic mean measured values are observed in the March equinox and December solstice, respectively**. The results also show that, even though overestimation of the modeled VTEC has been observed on most of the hours, all versions of the model are generally good to

estimate both the monthly and seasonal diurnal hourly VTEC values, especially in the early morning hours (00:00-03:00 UT or 03:00-06:00 LT). **It has also been shown that the IRI 2007 and IRI 2012 versions are generally better when the solar activity decreases; while IRI 2016 is better when the solar activity increases to capture the GPS VTEC values. In addition, the IRI 2012 version with IRI2001 option for the topside electron density shows the highest overestimation of the VTEC as compared to the other options.** All versions of the model do not also able to capture the effects resulting from storm.

Key words: GPS-VTEC; IRI- VTEC; GPS signal, solar maximum

1. Introduction

The energy transferred from the sun causes atoms and molecules existing in the atmosphere to undergo chemical reactions and become ionized (Kelley, 2009). This ionized and conductive region of Earth's atmosphere, extending from about 50 to 1000 km and possessing free electrons and positive ions generally in equal numbers in a medium that is electrically neutral, is termed as ionospher. The existence of these ions (plasma) in the ionosphere results in the possibility of radio communications over large distance by making use of one or more ionospheric reflections (Hunsucker and Hargreaves, 2003).

On the other hand, the ionosphere affects the electromagnetic waves that pass through it by inducing additional transmission time delay (Gao and Liu, 2002). Because of its dispersive character, electromagnetic signals (such as GPS signals) experience time delay (modulated codes) and advance (carrier phase) as they propagate through the ionosphere. This delay is directly proportional to the integral number of electrons in a unit cross-sectional area (usually referred to as total electron content, TEC) along the signal path extending from the satellite to the

receiver on the ground, and inversely proportional to the square of the frequency of propagation (Hofmann-Wellenhof et al., 1992; Misra and Enge, 2006). The dispersive ionosphere introduces a time delay in the 1.57542 GHz (L1) and 1.22760 GHz (L2) simultaneous transmissions from GPS satellites orbiting at 20,200 km (Hansen et al., 2000). The relative ionospheric delay of the two signals is proportional to the TEC. Time delay measurements of L1 and L2 frequencies can, therefore, be converted to TEC along the ray path from the receiver to the satellite (Lanyi and Roth, 1988). The GPS signals traverses the ionosphere carrying signatures of the dynamic medium and thus offers opportunities for ionospheric research. As a result, global and regional maps of ionospheric TEC can be produced using data from the worldwide network of the International GPS Service (Lanyi and Roth, 1988). The availability of TEC measurements is also important to the development of ionospheric models such as the International Reference Ionosphere, IRI (Bilitza, 2001). The International Reference Ionosphere (IRI) is an international project sponsored by the Committee on Space Research (COSPAR) and the International Union on Radio Science (URSI).

Using the GPS satellites and the IRI model, there have been so far several researches conducted globally in connection with the TEC variability and performance of the model over equatorial and low latitude regions**,** especially using IRI 2007 and IRI 2012 versions (e.g. Ezquer et al., 2014; Luhr and Xiong, 2010; Nigussie et al., 2013; Sethi et al., 2011; Olwendo et al., 2012a; Olwendo et al., 2012b). Nigussie et al., 2013, for instance, reported that IRI 2007 model overestimates the VTEC values over the East African equatorial regions. Using IRI 2007, Sethi et al., 2011, also showed that using IRI 2007 model with IRI 2001 option for the topside electron density highly overestimates the VTEC in all seasons and times over low and equatorial Indian regions**.** Olwendo et al. (2012a) also noted that seasonal average IRI 2007 TEC values were

higher than the GPS-TEC data for the period of 2009-2011 over different regions in Kenya. In addition, Olwendo et al. (2012b) reported that the IRI 2007 TEC is too high for all seasons except for the March equinox (where there seems to be good agreement between observation and model) during the lowest solar activity phase (2009-2010). Ezquer et al. (2014), using IRI 2012, noted that IRI 2012 predictions show significant deviations from experimental values during the period of 2008-2009 for a station placed at the southern crest of the equatorial anomaly in the American region. The report of Kumar (2016) on the validation of the IRI 2012 models for the global equatorial region also showed that the IRI 2012 model generally overestimated the observed VTEC over equatorial regions during the solar minimum year (2009) and solar maximum (2012) phases. Asmare et al. (2014) and Tariku, 2015a and Tariku, 2015b also attempted to see patterns in both the measured and modeled VTEC variations during the low and high solar activity phases employing different GPS stations and IRI 2012 model at various regions of Ethiopia. Asmare et al. (2014), for instance, showed that the IRI 2012 model entirely overestimates both monthly and seasonal VTEC values during phases of low solar activity. In addition, the model performance in estimating diurnal VTEC variations was found to be better during low solar activity phases than during high solar activity phases. In addition, the highest and the lowest values of the VTEC are observed in the equinoctial and the June solstice months, respectively during both the low and high solar activity phases. Abdu et al. (1996); Kakinami et al. (2012); Kumar et al. (2015) also attempted to describe the model's capacity to estimate the TEC using different versions of the model. **However, different findings show that the assessment of the improvement of the model performance from the relatively old to new versions for TEC estimation purpose in long lasting period is lacking over low latitude and equatorial regions, such as Ethiopia though the model has been steadily improved and**

arrived at the most recent version (IRI 2016). Hence, for a better improvement of the IRI model in estimating the variation of TEC, its performance has to be continuously tested, especially over the equatorial and low latitude regions, where the dynamics of the ionosphere is very complex. In addition, there are few researches conducted to test the performance of IRI 2016 model over the region. The model includes some new features that are supposed to enhance its performance in estimating different ionospheric parameters. For instance, the two new model options for the F2-peak height hmF2 and a better representation of topside ion densities at very low and high solar activities enable the model in estimating *hmf2* directly and no longer through its relationship to the propagation factor *M(3000)F2*. As a result, the new model options make the IRI 2016 model estimate evening peaks that was not possible in the old versions.

Thus, this study is mainly important to observe the TEC variation and the improvement of performance of the IRI model in estimating the TEC variation over low latitude African regions during the high solar activity phase (2013-2016) employing the GPS VTEC data inferred from different regions of Ethiopia. To observe the TEC variation and improvement of performance of the IRI model in estimating the TEC variation the latest versions (IRI 2007, IRI 2012 and IRI 2016) with NeQuick option for the topside electron density during the solar maximum phase have been considered. The prediction performance of the model has been tested by comparing the modeled TEC values with the GPS-TEC values recorded in the receivers.

2. Data description and analysis method

2.1. TEC from dual frequency GPS receiver

As different studies **(such as Ciraolo et al., 2007; Mannucci et al., 1998) show the GPS measurements are used to estimate the TEC along a ray path between a GPS satellite and receiver on the ground.** These GPS measurements can be recorded using either single or dual frequency GPS receivers. However, to eliminate ionospheric errors in the estimation of TEC dual frequency receivers are better **(Klobuchar, et al., 1996).** Moreover, by computing the differential phases of the code and carrier phase measurements, dual frequency GPS receivers can provide integral information about the ionosphere and plasma sphere (Ciraolo et al., 2007; Nahavandchi and Soltanpour, 2008). Hence, in this paper, the GPS-TEC data have been obtained from dual frequency receiver using pseudo-range and carrier phase measurements. The TEC inferred from the pseudo-range (P) measurement is given by:

$$TEC_P = \frac{1}{40.3}\left[\frac{f_1^{\,2} f_2^{\,2}}{f_1^{\,2} - f_2^{\,2}}\right](P_2 - P_1). \quad \textbf{(1)}$$

Similarly, the TEC from carrier phase measurement (Φ) is given as

$$TEC_\Phi = \frac{1}{40.3}\left[\frac{f_1^{\,2} f_2^{\,2}}{f_1^{\,2} - f_2^{\,2}}\right](\Phi_1 - \Phi_2), \quad \textbf{(2)}$$

where f_1 and f_2 can be related with the fundamental frequency, $f_o = 10.23MHz$

$$\begin{aligned} f_1 &= 154 f_o = 1575.42MHz, \\ f_2 &= 120 f_o = 1227.60MHz. \end{aligned} \quad \textbf{(3)}$$

As shown above, by cross correlating the f_1 and f_2 modulated carrier signals which are generally assumed to travel along the same path through the ionosphere, the GPS receiver obtains the time delay of the code and the carrier phase difference. **The TEC obtained from code pseudo-range measurements is free of ambiguity, but with relatively much noise. On**

the other hand, the TEC obtained from carrier phase measurements has relatively less noise, but it is ambiguous. Thus, linearly combining both code pseudo-range and carrier phase measurements for the same satellite pass is believed to increase the accuracy of TEC (Ciraolo et al., 2007; Gao and Liu, 2002; Klobuchar et al., 1996). This resultant absolute TEC is the GPS-derived STEC along the signal from the satellite to the receiver on the ground. To better characterize the TEC over a given receiver position and see the overall ionization of the Earth's ionosphere, the slant TEC (STEC) must be converted into equivalent vertical TEC (VTEC) at the mean ionospheric height, h_m=350 km (Mannucci et al., 1998; Norsuzila et al., 2008, 2009). Hence, the relationship between STEC and VTEC in terms of the zenith angle χ' at the Ionospheric Piercing Point (IPP) and the zenith angle χ at the receiver position can be given by:

$$VTEC = STEC\left(\cos\chi'\right), \tag{4}$$

where, .

$$\chi' = \arcsin\left[\frac{R_e}{R_e + h_m}\sin\chi\right]. \tag{5}$$

Substituting equation (5) into equation (4) and rearranging, we get

$$VTEC = STEC\left\{\cos\left[\arcsin\left(\frac{R_e}{R_e + h_m}\sin\chi\right)\right]\right\}. \tag{6}$$

Here, R_e is the radius of the Earth in kilometers.

2.2. TEC from the International Reference Ionosphere (IRI) model

153 The International Reference Ionosphere (IRI) is an international empirical standard
154 model used for the specification of ionospheric parameters. The model provides average values
155 of electron density, electron content, electron and ion temperature, and ion composition as a
156 function of height, location, local time, and sunspot number for magnetically quiet conditions
157 (Bilitza, 2001; Bilitza et al., 2014; Bilitza et al., 2017). To enhance the capacity of the model,
158 improvements have been made through the ingestion of all worldwide available data from
159 ground-based as well as satellite observations. As a result, a new version of the model (IRI 2016)
160 has been released in 2017 by incorporating some new input parameters that are supposed to
161 increase its capacity. The IRI 2016 model includes two new model options for the F2-peak
162 height hmF2 and a better representation of topside ion densities at very low and high solar
163 activities. The two new options are used in modeling *hmf2* directly and no longer through its
164 relationship to the propagation factor *M(3000)F2*. Thus, the new model options enable the IRI
165 2016 model to predict evening peaks that was not possible in the old versions. In addition, the
166 improvement of the ion composition model in the topside ionosphere can lower the transition
167 height from close to 1000 km down to almost 600 km in the new version of the model. A number
168 of smaller changes have also been made concerning the use of solar indices and the speed-up of
169 the computer program (Bilitza et al., 2017). For a given location, time and date, like the previous
170 versions of the model, IRI-2016 model provides the monthly averages of ionospheric parameters
171 (such as TEC) in the altitude range from about 50–2000 km (Bilitza et al., 2017;
172 http://IRImodel.org.). For more information, see the model web site
173 **(**http://omniweb.gsfc.nasa.gov/vitmo/iri-vitmo.html**)** that was accessed for the period of 25-
174 30/01/2018.
175

176 *2.3. Data sources and method of analysis*

177 The data required for both the experimental and model were obtained from Ethiopian **sites**
178 shown in Figure 1 during the solar maximum (2013-2016) phase. Table 1 also shows the GPS
179 receiver locations used for the study. The raw GPS data for the described station were obtained
180 from the University NAVSTAR Consortium (UNAVCO web site, http://www.unavco.org/). The
181 data gained from this web site have two forms: observation and navigation data in which both of
182 them are zipped. To use the data for the desired purpose, the GG software (GPS-TEC calibrating
183 software) was used to process the required data in five minutes interval and an elevation cut-off
184 10^{o}.

185 To get the required results, the corresponding modeled VTEC values were inferred from the
186 latest versions of the model (IRI 2007, IRI 2012 and IRI 2016) that include some latest input
187 parameters which are supposed to improve the capacity of the model in estimating ionospheric
188 parameters. The online IRI versions of the model were obtained from
189 http://omniweb.gsfc.nasa.vitmo.html. To get the VTEC values, the year, date, month, location,
190 the hour profile, the upper boundary altitude (2000 km), daily sunspot number and **F10.7 cm**
191 **flux**, topside electron density options (NeQuick, IRI01, IRI2001), CCIR for F peak model, and
192 ABT-2009 for bottomside thickness option were used as the input parameters,.

193 In order to observe the pattern of the hour-to-hour variability of VTEC, the mean monthly
194 and seasonal hourly GPS TEC and the corresponding IRI TEC data have been used during the
195 period of 2013-2016. To see the monthly and seasonal arithmetic mean VTEC variation and the
196 model performance, the hour-to-hour measured and modeled VTEC values have been
197 correspondingly added and averaged for the whole days in each month and season. The seasons
198 could be classified as December solstice (November, December and January), March equinox

(February, March and April), June solstice (May, June and July) and September equinox (August, September and October). For a better understanding on the performance of the model, the absolute differences between the monthly and seasonal GPS VTEC and the corresponding IRI VTEC values have been determined. The differences have been calculated by subtracting the experimental VTEC values from the model. In order to clearly see the validation of the model, the absolute differences between the IRI VTEC and GPS VTEC in all the monthly and seasonal variations were determined. In addition, the percentage differences between the IRI VTEC and GPS VTEC for the arithmetic monthly and seasonal VTEC variations have also been determined.

3. Results and discussion

3.1. Diurnal monthly and seasonal variation of VTEC and performance of the IRI model

The results of the variations of the monthly and seasonal hourly VTEC are displayed in Figs 2-7. As observed in the figures, both the measured and modeled VTEC values start decreasing in the nighttime hours and become minimum after midnight hours (on average at 03:00 UT or 06:00 LT) and start increasing again to attain their peak values in the time interval of about 09:00-13:00 UT or 12:00-16:00 LT). Moreover, in some hours, the modeled VTEC values (in all versions) are in a good agreement with the measured (GPS VTEC) values, especially in the nighttime hours (00:00-03:00 UT or 03:00-06:00 LT). On the other hand, all versions of the model tend to underestimate the VTEC values during the daytime hours (09:00-13:00 UT or 12:00-16:00 LT). **Overestimations are also observed, especially in using IRI 2001 option for IRI 2012 model in 2013-2014 (see Figs. 4 and 5) and using IRI 2016 model in 2016 (see Fig. 7). In the year 2013-2016, the highest underestimation (by about 30 TECU) and highest overestimation (by about 20 TECU) are observed in the March equinox in 2015**

(using IRI 2016 model) and June solstice in 2014 (using IRI 2012 model with IRI 2001 option), respectively at about 12:00 UT (15:00 LT). However, IRI 2007 and IRI 2012 are generally better to capture the VTEC values as the solar activity decreases; while, IRI 2016 version is generally better when the solar activity increases. Moreover, the IRI 2012 version with NeQuick and IRI01-Corr gives hourly VTEC variation having closer hourly VTEC values (see Figs. 4 and 5). The mismodelings observed in both cases may be due to the difference in the model and experimental slab-thickness as noted by different findings (e.g. Nigussie et al., 2013; Rios et al., 2007). For instance, Rios et al. (2007) using the IRI 2001 model, showed that IRI predicted slab thickness is higher than the measured values except between (10:00-14:00 LT) which can attribute to VTEC fluctuations in similar trend. This is almost consistent with the result determined in this work. Using IRI 2007 model, Nigussie et al. (2013) also suggested similar possible reason for the discrepancy between the model and the experimental VTEC values. It could also be resulting from poor estimation of the hmF2 and foF2 from the coefficients, which in turn may result in poor estimation of VTEC by the IRI model (e.g. Chakraborty et al., 2014; Kumar et al, 2015). The underestimation of the IRI VTEC values by the GPS VTEC values may also attribute to the enhancement of the plasmaspheric electron content above 2000 km during the daytime hours **(Coisson et al., 2008; Aggarwal, 2011; Venkatesh et al., 2011).**

Moreover, the maximum peak of both the measured and modeled VTEC values are generally observed in the equinoctial months; while, the minimum peak values are observed in the June solstice months (see Fig. 2-7). For instance, over Arba Minch station (see Figs. 2 and 3), the highest and lowest peak measured monthly VTEC values of about 80 and 40 TECU are observed in March and July, respectively in 2015. Similarly, the highest and lowest peak

245 modeled monthly VTEC values of about 55 and 41 TECU are observed in April and July,
246 respectively in using IRI 2007 model with NeQuick option for the topside electron density. In
247 addition, the highest and lowest peak measured seasonal VTEC values of are observed in the
248 March equinox and June solstice, respectively in 2015. The highest and lowest peak modeled
249 seasonal VTEC values of about 54 and 43 TECU are also observed in the March equinox and
250 June solstice, respectively when using IRI 2007 model with NeQuick option for the topside
251 electron density over Arba Minch station (see Fig. 6). In addition, in using IRI-2012 model with
252 IRI2001 option for the topside electron density, the highest and lowest peak measured seasonal
253 VTEC values of about 70 and 40 TECU are observed in the March equinox and June solstice,
254 respectively over Ambo station in 2014. Similarly, the highest and lowest peak modeled seasonal
255 VTEC values of about 74 and 60 TECU are observed in the March equinox and June solstice,
256 respectively in 2014 when using the same version of the model (IRI 2012) with IRI2001 option
257 (see Fig. 5). **The overall results show that, in the year 2013-2016, the highest peak measured**
258 **VTEC values of about 80 TECU is observed in the March equinox in 2015.**
259 It is known that, in general, electron population in the ionosphere is mainly controlled by
260 solar **photoionization** and recombination processes (Wu et al., 2004). Thus, for the equinoctial
261 months, as the subsolar point is around the equator where the **eastward** electrojet associated
262 electric field is often largest, it would be speculated that the peak photoelectron abundance and
263 intense eastward electric field will be set up in the described region. On the contrary, for solstice
264 months photoelectrons at the equator decrease as the **subsolar** point moves to higher latitudes.
265 Moreover, the change of direction of neutral wind may account for the highest VTEC values in
266 the equinoctial months and lowest values in the June solstice months. A meridional component
267 of neutral wind blows from the summer to the winter hemisphere that is able to reduce the

ionization crest value during summer solstice as it blows in an opposite direction to the plasma diffusion process originating from the magnetic equator. Thus, in equinoxes meridional winds blowing from the equator to polar regions may attribute to a high ionization crest value. Hence, a seasonal effect on the crest should be expected with the crest maximum at the equinoxes and minimum in the summer season or June solstice (Bhuyan and Borah, 2007; Wu et al., 2004), which is consistent with the result of this work.

3.2. *Arithmetic mean of monthly and seasonal variations of VTEC and performance of the IRI model*

The results of the arithmetic mean monthly and seasonal VTEC variations are given in Figures 8-11. The results show that both the measured and the modeled arithmetic mean VTEC have generally the highest and lowest values in the equinoctial and June solstice months. For example, the highest and lowest measured arithmetic mean monthly VTEC values of about 38 and 18 TECU are observed in April and July, respectively in 2014 over Ambo station (see the left top panel of Fig. 9). The seasonal measured arithmetic mean VTEC variation also shows the highest and lowest values of about 37 and 21 TECU in the March equinox and June solstice, respectively in 2014 (see the left bottom panel of Fig. 9). In addition, the highest and lowest seasonal measured VTEC values of about 36 and 23 TECU are observed in the March equinox and June solstice, respectively over Arba Minch station in 2015. The highest and lowest seasonal modeled arithmetic mean VTEC values of about 32 and 24 TECU are also observed in the March equinox and June solstice, respectively when using IRI 2007 version (see the left bottom panels of Fig. 10). On the other hand, the highest and lowest measured monthly VTEC values are observed in November and February, respectively in 2013. Similarly, the highest and lowest

measured seasonal VTEC values are observed in the December solstice and March equinox, respectively (see the left top and bottom panels of Fig. 8). But, the highest and lowest modeled arithmetic mean seasonal VTEC values are observed in the March equinox and June, respectively in 2013 when using IRI 2001 option for the topside electron density (see the left top panel of Fig. 8). In **the year 2013-2014, using the IRI 2012 model with IRI2001 option for the topside electron density shows the highest overestimation as compared to NeQuick and IRI01-Corr options. As shown in the Figures (see the right top and bottom panels of Figs. 8 and 9), the highest monthly and seasonal overestimations are observed in July (by about 130%) and the June solstice (by about 100%) in 2014. On the other hand, the IRI 2012 version with NeQuick and IRI01-Corr option relatively gives VTEC having closer values (see Figs 8 and 9). Moreover, the IRI 2016 version shows overestimation of the VTEC as compared to others (IRI 2007 and IRI 2012), especially when the solar activity decreases.** For instance, the highest monthly and seasonal deviations of about 25% and 20% are observed between the modeled and corresponding measured values in September and the June solstice, respectively when IRI 2016 version is used (see the top and bottom right panels of Fig. 10).

3.3 Storm Time VTEC variation and performance of the IRI model

To see the VTEC variation and performance of the IRI model during storm time condition, the magnetic storm day (with **Dst index maximum incursion of about -222nT**) which occurred on March 17, 2015 as observed over Arba Minch station was considered **(see Fig. 12).** To better see the effect of the storm on the GPS VTEC and IRI VTEC, the pattern of the VTEC fluctuations in **the initial phase (16/03/2015), main phase (17/03/2015)** and in the recovery phase (18/03/2015) of the storm was considered. As shown in Fig. 13, the GPS-VTEC values show

significant fluctuation that indicates the occurrence of storm. On the other hand, the model VTEC values (IRI 2007, IRI 2012 and IRI 2016 VTEC) don't show any change when the storm model is "on" and "off" (see Figs.13a-13c and Figs.13d-13f). As shown in the figures, the mode VTEC values in all the three days follow almost similar pattern; they generally tend to underestimate the VTEC values (mostly after 08:00 UT or 11:00 LT) and remain smooth during the storm. This shows that the model does not respond to the effects resulting from storm. **The IRI 2016 VTEC values are also smaller than those of the IRI 2007 and IRI 2012 VTEC values in the initial, main and recovery phase of the storm.** In addition, enhancement of GPS TEC is observed as we proceed from the initial to the recovery phase of the storm. As shown in the figure, a peak VTEC value of about 65 TECU being observed in the initial phase increases to about 75 TECU in the recovery phase of the storm. This may be resulted from particle transport and the prompt penetration of high latitude electric fields (PPEFs) to lower latitude which travel equator ward with high velocities during the storm (Malik et al., 2010; Tsurutani et al., 2004; Sobral et al., 2001)**. As the findings show, the dayside ionospheric storms resulting from PPEFs are characterized by transport of near-equatorial plasma to higher altitudes and latitudes, producing a giant plasma fountain. Hence, if the electric field penetrates into the dayside equatorial ionosphere, the plasma is convected toward higher altitudes, forming a giant plasma fountain. At these higher altitudes, the recombination rates are longer than for lower altitudes. On the other hand, solar photoionization at lower altitudes simultaneously continues to occur. This photoionization process will replace the uplifted plasma resulting in an overall increment of TEC.**

4. Conclusions

Because of the unique geometry of the geomagnetic field near the magnetic equator and low latitude regions (such as Ethiopia), the signal propagation system through the ionosphere is largely affected by the accumulation of electrons (TEC). Hence, in this study, the VTEC variation and the improvement of performance of the IRI model over the equatorial and low latitude regions has been studied employing the GPS and IRI techniques during the period of 2013-2016. **The results reveal that the highest and lowest measured and modeled VTEC values are mostly observed in the equinoctial and June solstice months, respectively. However in 2013, the lowest and highest measured seasonal VTEC values are observed in the March equinox and December solstice, respectively. In the year 2013-2016, the maximum seasonal arithmetic mean measured VTEC values are observed in the March equinox except in 2013 in which the minimum and maximum being observed in the March equinox and December solstice, respectively.** In addition, though overestimation of the modeled VTEC has been observed on most of the hours, the model is generally good to estimate the diurnal hourly VTEC values mostly just after midnight hours (00:00-03:00 UT or 03:00-06:00 LT). It has also been shown that the model (IRI 2012) generally overestimates both the arithmetic mean of the monthly and seasonal hourly VTEC values, with the highest overestimation being observed in using IRI2001 option in 2013-2014. The overall results show that using NeQuick option for the topside electron density is generally better than other topside options for TEC estimation by IRI model. In general, the model does not show good improvements from version IRI 2007 to IRI 2016 in the TEC estimation over equatorial and low latitude regions. **However, the IRI 2007 and IRI 2012 versions are generally better to respond to the decrement of the VTEC values when the solar activity decreases; while IRI 2016 version is generally better to capture the measured VTEC values when the solar**

activity increases. Moreover, all versions of the model do not respond to the effects resulting from storm. Hence, further improvements have to be made on the model for the betterment of its performance in estimating the VTEC over the equatorial and low latitude regions.

Author contribution

All the required issues for the manuscript are prepared by the corresponding author, Yekoye

Competing interests

The corresponding author declares that he has no conflict of interest.

Acknowledgements

The data of daily sunspot number, GPS, Dst index and IRI model for this paper are freely available at: http://www.sidc.be/sunspot-data/,http://facility.unavco.org/data/dai2/app/dai2., http://wdc.kugi.kyoto-u.ac.jp/dst_final/201401/index.html and (http://omniweb.gsfc.nasa.gov/vitmo/iri vitmo.html), respectively. Hence, the author is very grateful to UNAVCO, NOAA, World Data Center (Kyoto University) and NASA for donating their free GPS, daily sunspot number, Dst index and online IRI model data, respectively.

References

Abdu, M.A., Batista, I.S.,Souza JR.(1996); An overview of IRI-observational data comparison in American (Brazilian) sector low latitude ionosphere. Adv Space Res 18(6):13-22.

Aggarwal, M. (2011); TEC variability near northern EIA crest and comparison with IRI model, Adv. Space Res., 48(7), 1221–1231, doi:10.1016/j. asr.2011.05.037

Asmare Y., Tsgaye, K., Melssew, N. (2014); Validation of IRI-2012 TEC model over Ethiopia during solar minimum (2009) and solar maximum (2013) phases. Adv Space Res, 1582-1594, http://dx.doi.org/10.1016/j.asr.2014.02.017.

Bhuyan, P.K., Borah,R.R. (2007); TEC derived from GPS net work in India and comparison with IRI. Advances in Space Research: The Official Journal of the Committee on Space Research (COSPAR) 39, 830-840.

Bilitza, D. (2001); International reference ionosphere 2000. Radio Sci. 36(2), 261-275.

Bilitza, D., D. Altadill, Y. Zhang, C. Mertens, V. Truhlik, P. Richards, L. McKinnell, and B. Bodo Reinisch, (2014); The International Reference Ionosphere 2012 – a model of international collaboration, J. Space Weather Space *Clim*., 4, A07, DOI: 10.1051/swsc/2014004

Bilitza1, D, D. Altadill, V. Truhlik, V. Shubin, I. Galkin, B. Reinisch, X. Huang (2017**);** International Reference Ionosphere 2016: from ionospheric climate to real-time weather predictions, Space Weather, DOI: 10.1002/2016SW001593.

Chakraborty,M., Kumar, S., Kumar, B., Guha, A.(2017); Latitudinal characteristics of GPS derived ionospheric TEC: a comparative study with IRI 2012 model, Annals of Geophysics, 57 (5), A0539; doi: 10.4401/ag-6438.

Ciraolo, L., F. Azpilicueta, C. Brunini, Meza, A. and S. M. Radicella (2007); Calibration errors on experimental slant total electron content (TEC) determined with GPS, *J.*, *Geodesy*, 81, 111–120

Coisson P., S. M. Radicella, L. Ciralo, R. Leitinger, and B. Nava (2008), Global validation of IRI TEC for high and medium solar activity conditions, Adv. Space Res., 42, 770–775.

406 Ezquer, R.G., López, J.L., Scidá, L.A., Cabrera, M.A., Zolesi, B., Bianchi, C., Pezzopane M.,
407 Zuccheretti, E., Mosert, M. (2014); Behaviour of ionospheric magnitudes of F2 region over
408 Tucumán during a deep solar minimum and comparison with the IRI 2012 model
409 predictions. J. Atmos. Sol-Terr. Phys. 107:89-98.
410 Gao, Y.,Liu,Z.Z. (2002); Precise ionospheric modeling using regional GPS network data, Journal
411 of Global Positioning system, vol. 1, No. 1:18-24.
412 Hansen, A., Blanch,J., T. Walter, T. (2000); Ionospheric correction analysis for WAAS quiet and
413 stormy, in Proceedings of the 13th International Technical Meeting of the Satellite Division
414 of The Institute of Navigation ION GPS, Salt Lake City, Utah, 19-22.
415 Hofmann-Wellenhof, B., Lichtenegger, H., Collins, J. (1992); Global Positioning System Theory
416 and Practice. Springer-VerlagWien, New York.
417 Hunsucker, R.D. and Hargreaves, R.D. (2003); The high-latitude ionosphere and its effects on
418 radio propagation, Cambridge Univ. Press, UK.
419 Kakinami, Y., Liu, J.Y., Tsai, L.C. (2012); A comparison of a model using the FORMOSAT-
420 3/COSMIC data with the IRI model. Earth, Planets, Space, 64:545-551.
421 Kelley, M.C. (2009); The Earth's Ionosphere: Plasma Physics and Electrodynamics,
422 Second Edition. Elsevier Inc., New York.
423 Kumar, S., Tan, E., Murti. D. (2015); Impacts of solar activity on performance of the IRI-2012
424 model predictions from low to mid latitudes. Earth, Planets, Space, 67:42.
425 doi:10.1186/s40623-015-0205-3
426 Kumar, S. (2016); Performance of IRI-2012 model during a deep solar minimum and a
427 maximum year over global equatorial regions, J. Geophys. Res., Space Physics, 121,
428 doi:10.1002/2015JA022269.

Klobuchar, J.A., Parkinson, B.W., Spilker, J.J. (1996); Ionospheric effectson GPS, in: Global Positioning System: Theory and Applications, American Institute of Aeronautics and Astronautics,Washington, DC.

Lanyi, G.E. and Roth, T. (1988); A Comparison of Mapped and Measured Total Ionospheric Electron Content Using Global Positioning System and Beacon Satellite Observations. Radio Science, Vol. 23, No. 4, pp. 483-492.

Luhr, H., Xiong, C. (2010**);** IRI-2007 model overestimates electron density during the 23/24 solar minimum, Geophysical Research Letters, Space Sciences, 37(23), **https://doi.org/10.1029/2010GL045430**

Mannucci, A.J., Wilson, B.D., Yuan, D.N., Ho, C.H., Lindqwister, U.J.,Runge, T.F. (1998); A global mapping technique for GPS-derived ionospheric total electron content measurements. Radio Sci. 33, 565-582, http://dx.doi.org/10.1029/97RS02707.

Malik, Rakhee, Sarkar, Shivalika, Mukherjee, Shweta, Gwal, A.K (2010); Study of ionospheric variability during geomagnetic storms. J. Ind. Geophys. Union 14 (1), 47-56.

Misra, P., Enge, P. (2006); Global Positioning System: Signals, Measurements and Performanc 2nd ed., Ganga-Jamuna Press, Lincoln, MA01773.

Nahavandchi, H., Soltanpour, A. (2008); Local ionospheric modeling of GPS code and carrier phase observation, vol. 40,309, pp.271-284.

Nigussie, M., Radicella, S.M., Damtie, B.,Nava,B., Yizengaw, E., Groves, K. (2013); Validation of the NeQuick 2 and IRI-2007 models in East-African equatorial region. J. Atmos. Sol-Terr. Phys., http://dx.doi.org/10.1016/j.jastp.2013.04.016.

Norsuzila, Y., Ismail, M., Abdullah M. (2008); Investigation of the GPS signals ionospheric correction: Ionospheric TEC prediction over equatorial region, IEEE International

453 Conference on Telecommunications and Malaysia International Conference on
454 Communications (ICT-MICC 2007); Penang, Malaysia. 294-298, 14-17.
455 Norsuzila, Y., Mardina, A., Mohamod, I., Azami, Z. (2009); Model validation for Total
456 electron coneten (TEC) at equatoria region, Europian Journal of scientific research vol.28,
457 No.4, pp 642-648.
458 Olwendo, O.J., Baki, P., Mito, C., Doherty, P. (2012a); Characterization of ionospheric
459 GPS total electron content (GPS TEC) in low latitude zone over the Kenyan region
460 during a very low solar activity phase. J. Atmos. Sol-Terr. Phys., 84-85:52-61.
461 Olwendo, O.J., Baki, P., Mito, C., Doherty,O. (2012b); Comparison of GPS TEC variations with
462 IRI-2007 TEC prediction at equatorial latitudes during a low solar activity (2009-2011)
463 phase over the Kenyan region. J Adv Space Res.
464 http://dx.doi.org/10.1016/j.asr.2012.08.001.
465 Rios, V.H., Medina, C.F., Alvarez, P. (2007); Comparisons between IRI predictions and
466 digisonde measurements at Tucuman. J. Atmos. Sol. Terr. 69, 569-577..
467 Sobral, J. H., M. A. Abdu, C. S. Yamashita, W. D. Gonzalez, A. C. de Gonzalez, I. S. Batista, C.
468 J. Zamlutti, and B. T. Tsurutani (2001); Responses of the low-latitude ionosphere to very
469 intense geomagnetic storms, J. Atmos. Sol. Terr. Phys., 63, 965–974, doi:10.1016/S1364
470 6826(00)00197-8.
471 Sethi, N., Dabas, R., Sarkar, S. (2011); Validation of IRI 2007 against TEC observations during
472 low solar activity over Indian sector.
473 Tariku Y.A. (2015a); Patterns of GPS-TEC variation over low-latitude region (African sector)
474 during the deep solar minimum (2008 to 2009) and solar maximum (2012 to 2013) phases.
475 Earth, Planets, Space 67:35. doi:10.1186/ s40623-015-0206-2.

476 Tariku, Y.A. (2015b); TEC prediction performance of the IRI-2012 model over Ethiopia during
477 the rising phase of solar cycle 24 (2009-2011), Earth, Planets and Space (2015) 67:140
478 DOI 10.1186/s40623-015-0312-1.
479 Tsurutani, B., et al. (2004), Global dayside ionospheric uplift and enhancement associated with
480 interplanetary electric fields, J. Geophys. Res., 109, A08302, doi: 10.1029/2003JA010342.
481 Venkatesh, K., P. V. S. Rama Rao, P. L. Saranya, D. S. V. V. D. Prasad, and K. Niranjan (2011),
482 Vertical electron density and topside effective scale height (HT) variations over the Indian
483 equatorial and low latitude stations, Ann. Geophys., 29, 1861–1872, doi:10.5194/angeo-29-
484 1861-2011.
485 Wu, C.C., Fry, C.D., Liu, J.Y., Liou, K., Tseng, C.L. (2004); Annual TEC variation in the
486 equatorial anomaly region during the solar minimum: September, 1996-August 1997., J.
487 Atmos. Terr. Phys., 66:199-207.
488
489 Figures

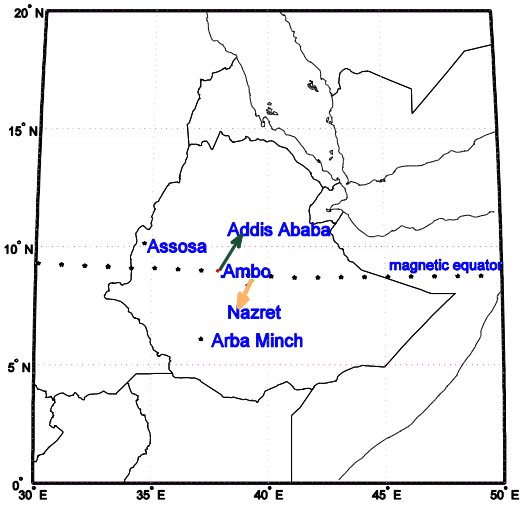

490
491 Figure 1: Location of GPS receivers used for the study

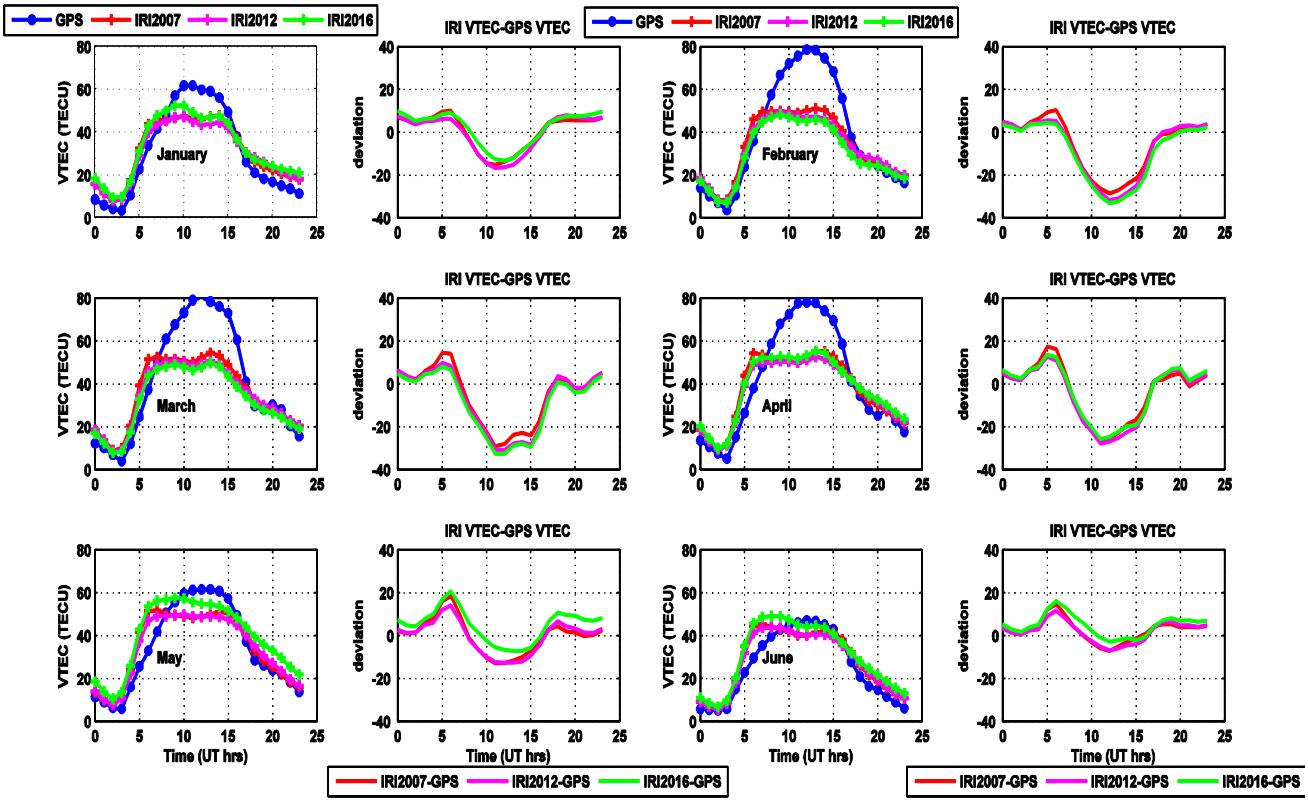

492

493 Figure 2: A graph to illustrate diurnal monthly VTEC variation and performance of the IRI

494 model over Arba Minch station during the period of January-June in 2015

495

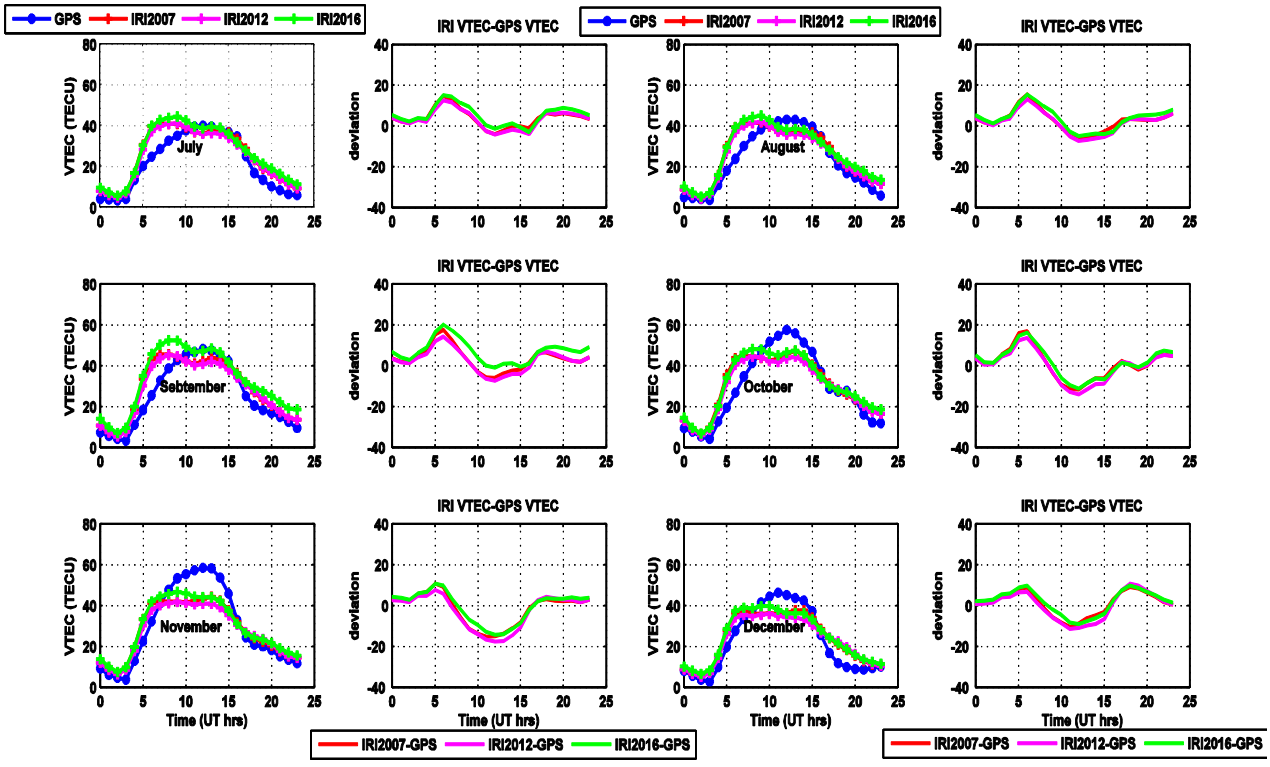

Figure 3: A graph to illustrate diurnal monthly VTEC variation and performance of the IRI model over Arba Minch station during the period of July-December in 2015

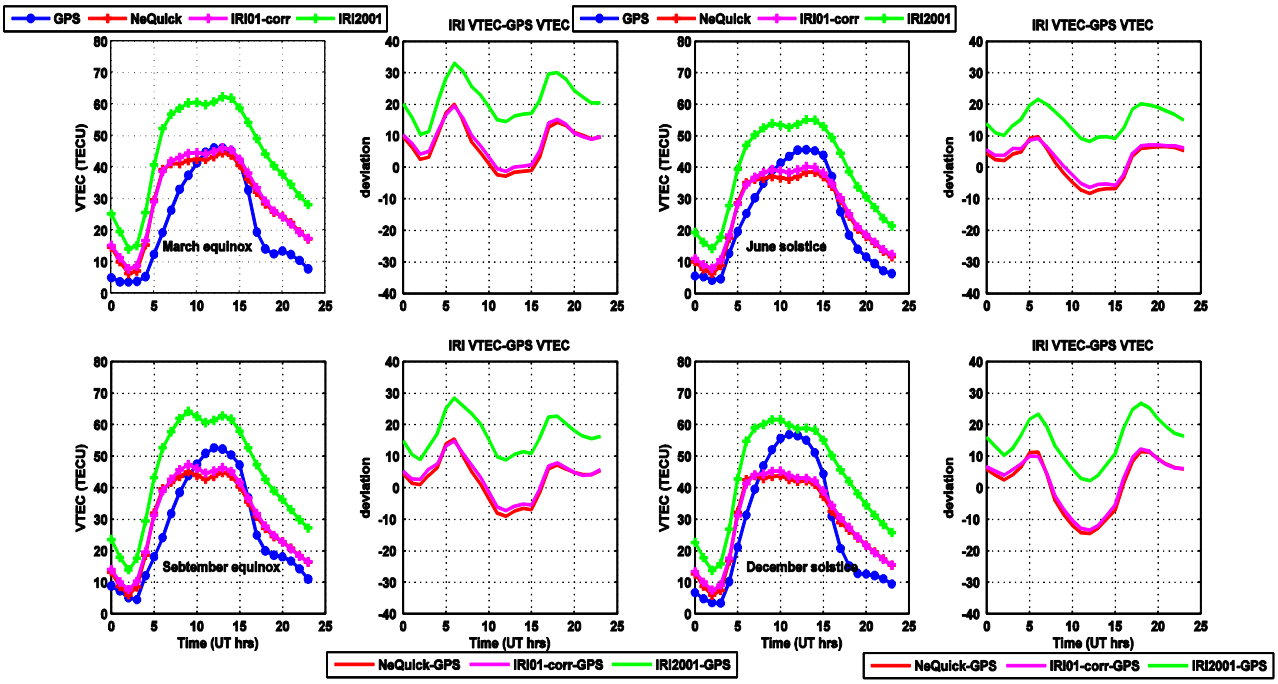

Figure 4: A graph to illustrate diurnal seasonal VTEC variation and performance of the IRI-2012 model over Ambo station during the period of 2013

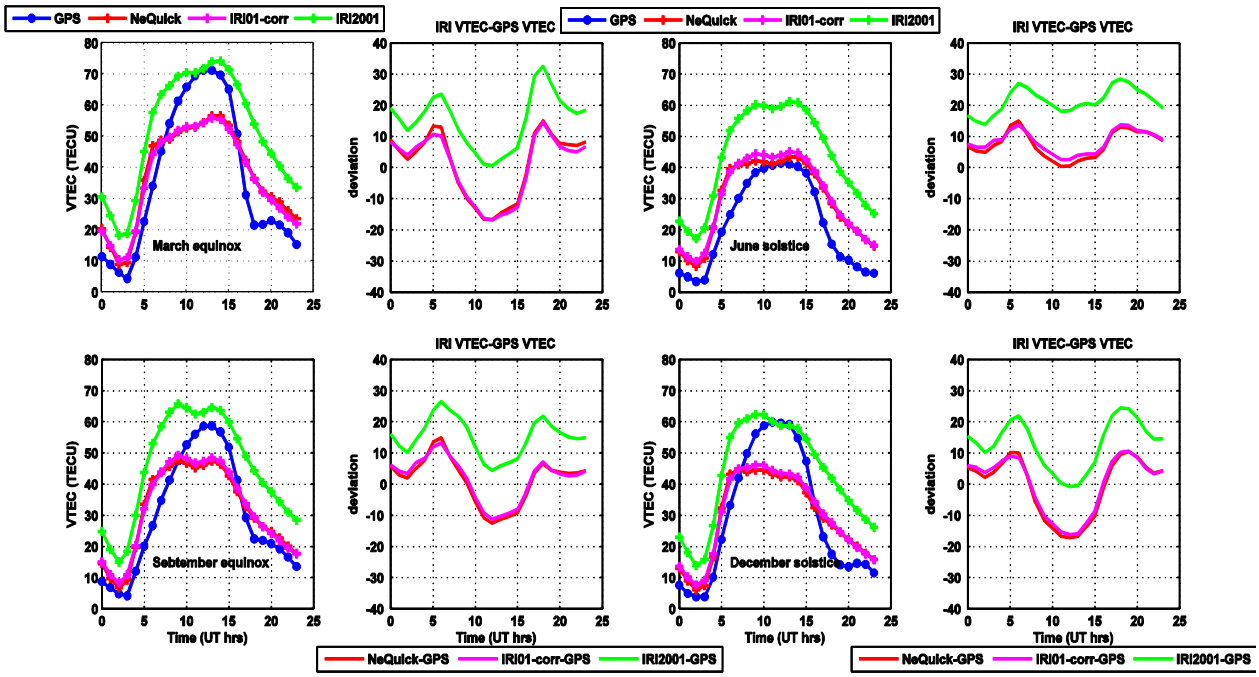

Figure 5: A graph to illustrate diurnal seasonal VTEC variation and performance of the IRI-2012 model over Ambo station during the period of 2014

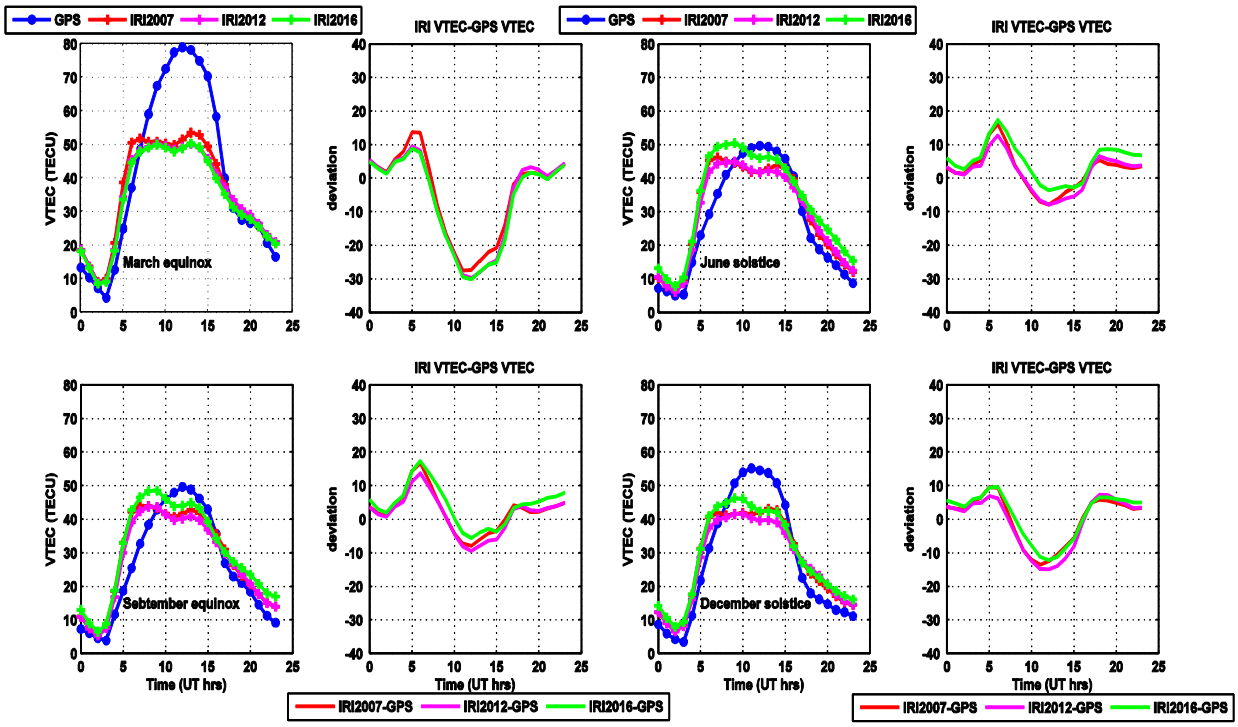

506

507

508 Figure 6: A graph to illustrate diurnal seasonal VTEC variation and performance of the IRI

509 model over Arba Minch station during the period of 2015

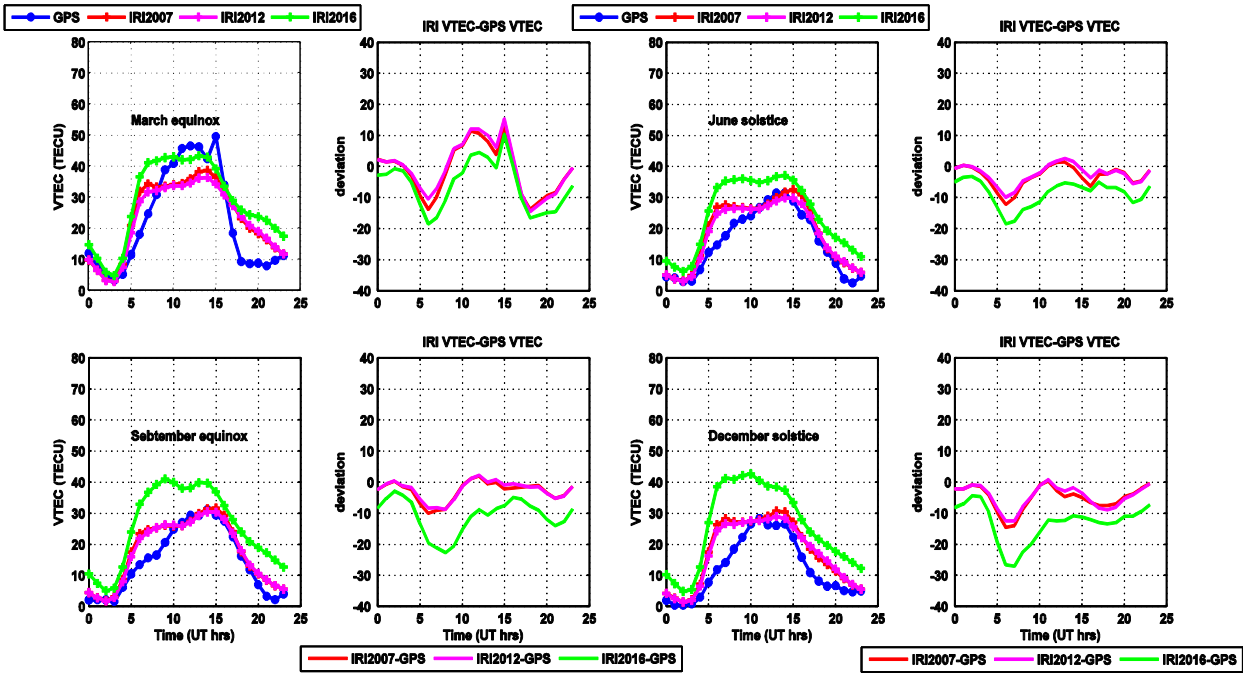

510

Figure 7: A graph to illustrate diurnal seasonal VTEC variation and performance of the IRI model over Asosa station during the period of 2016

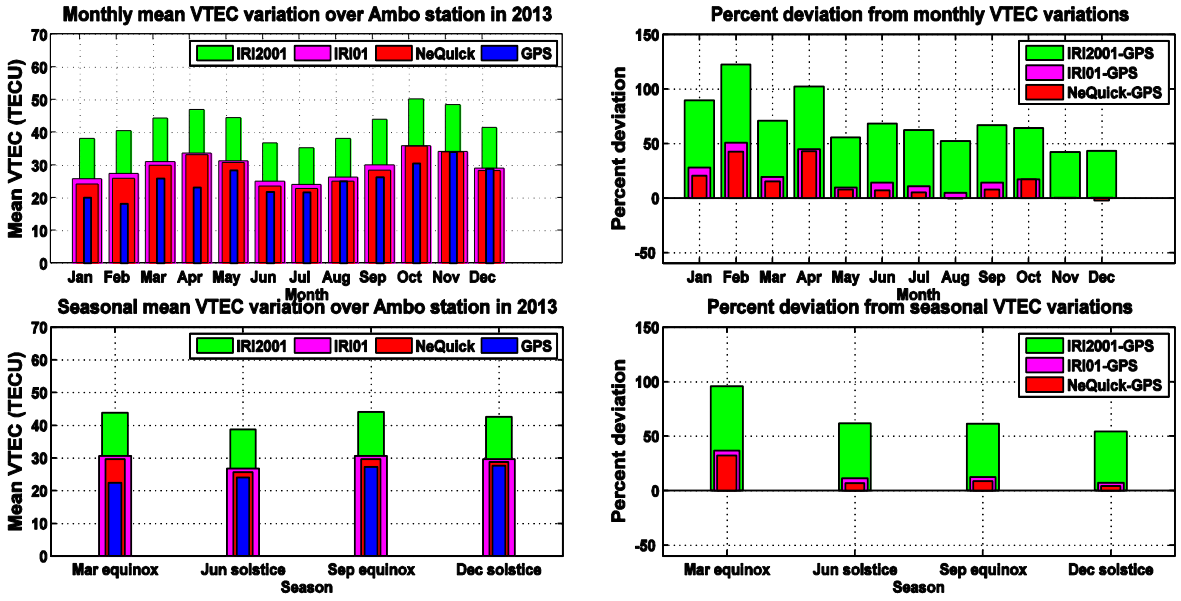

Figure 8: A graph to illustrate the arithmetic mean monthly and seasonal VTEC variation and performance of the IRI-2012 model over Ambo station during the period of 2013

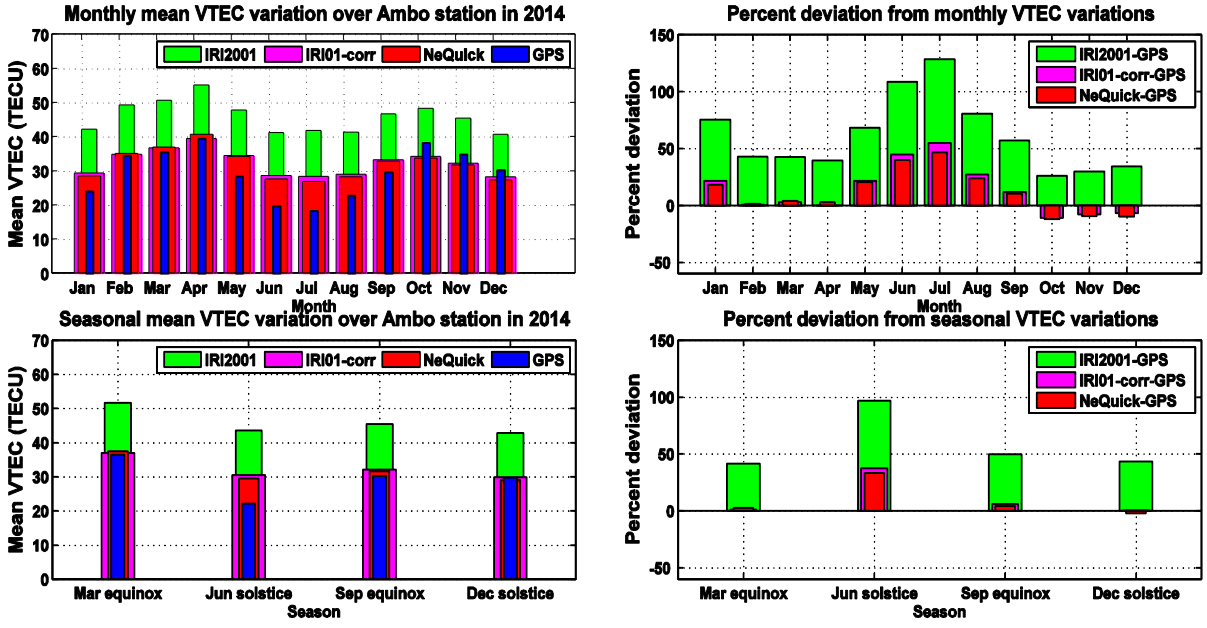

Figure 9: A graph to illustrate the arithmetic mean monthly and seasonal VTEC variation and performance of the IRI-2012 model over Ambo station during the period of 2014

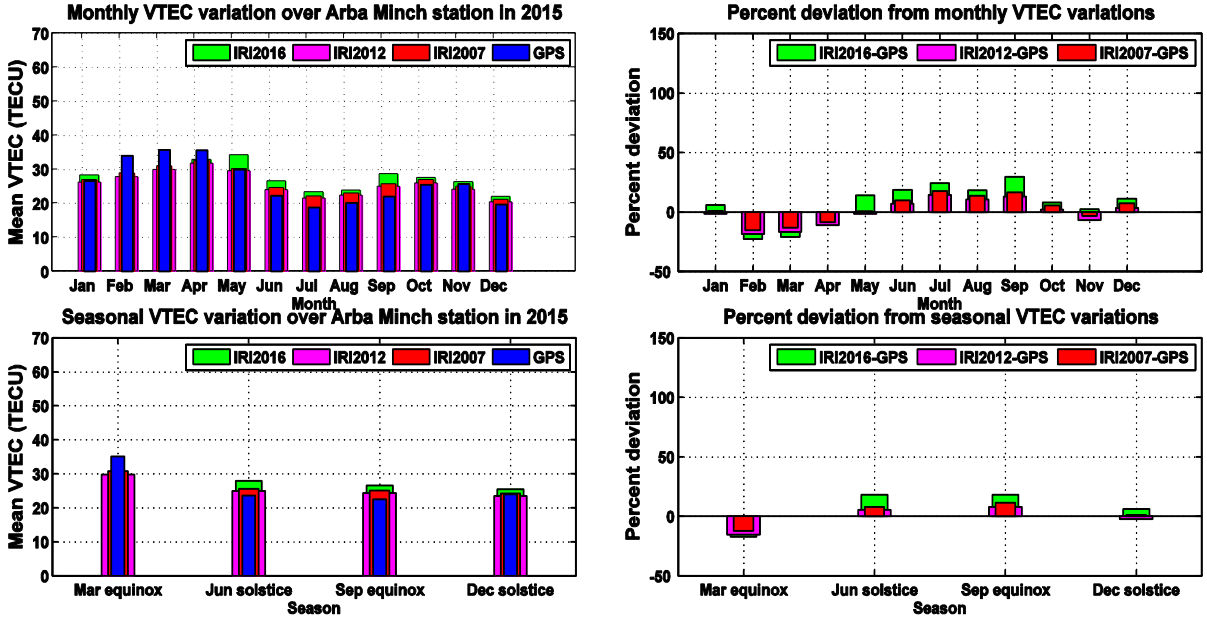

Figure 10: A graph to illustrate the arithmetic mean monthly and seasonal VTEC variation and performance of the IRI model over Arba Minch station during the period of 2015

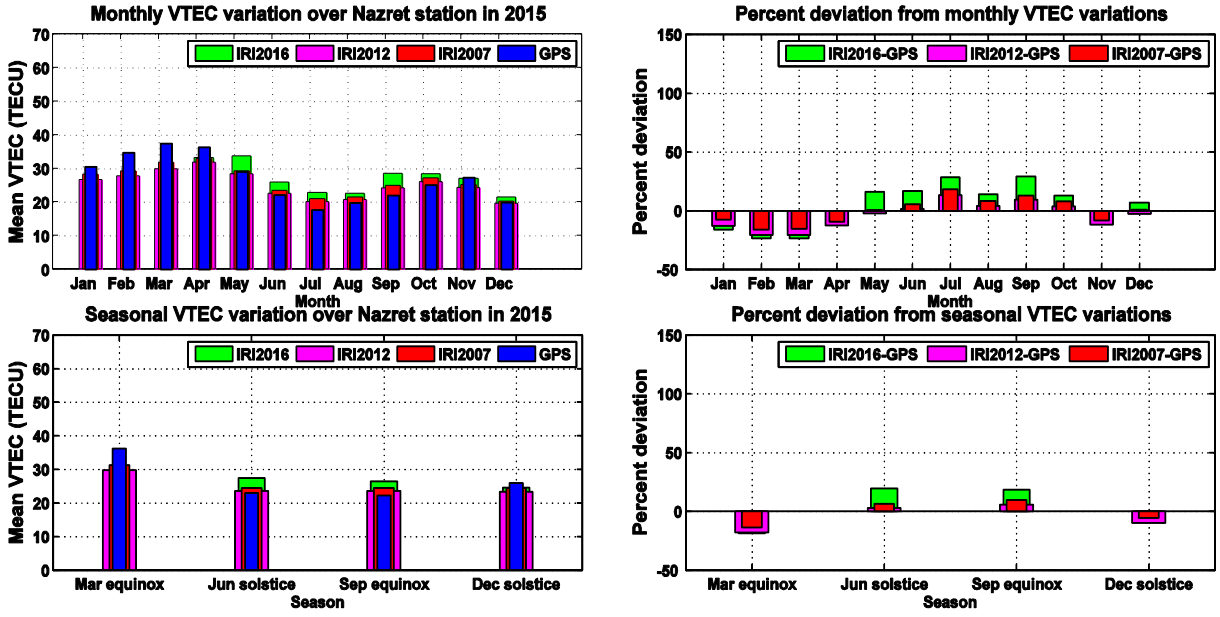

Figure 11: A graph to illustrate the arithmetic mean monthly and seasonal VTEC variation and performance of the IRI model over Nazret station during the period of 2015

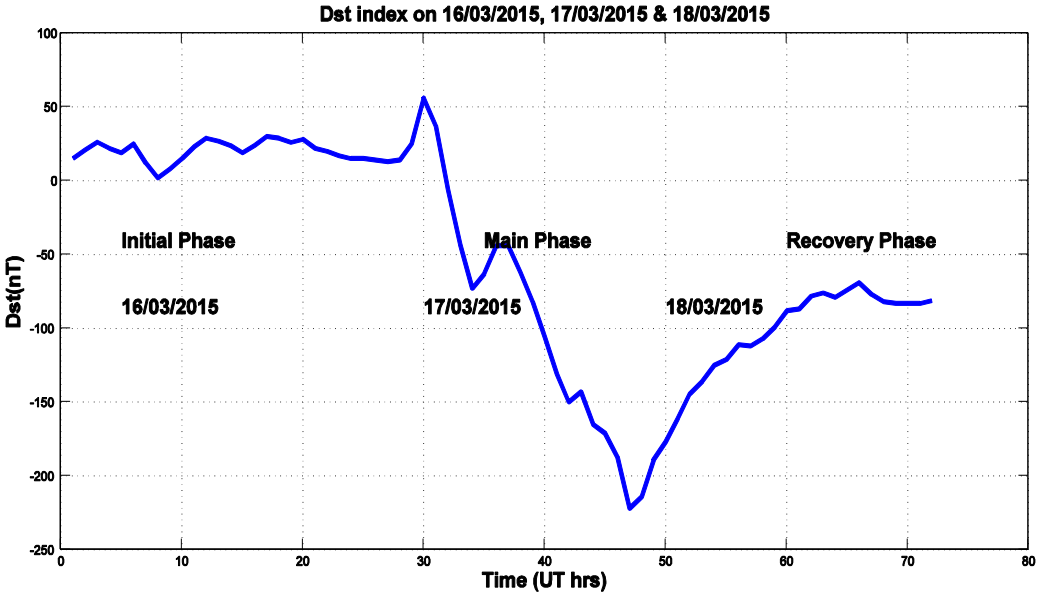

Figure 12: Dst index on 16/03/2015, 17/03/2015, and 18/03/2015 as observed over Arba Minch station during the period of 2015 (data source for Dst index: World Data Center, Kyoto University).

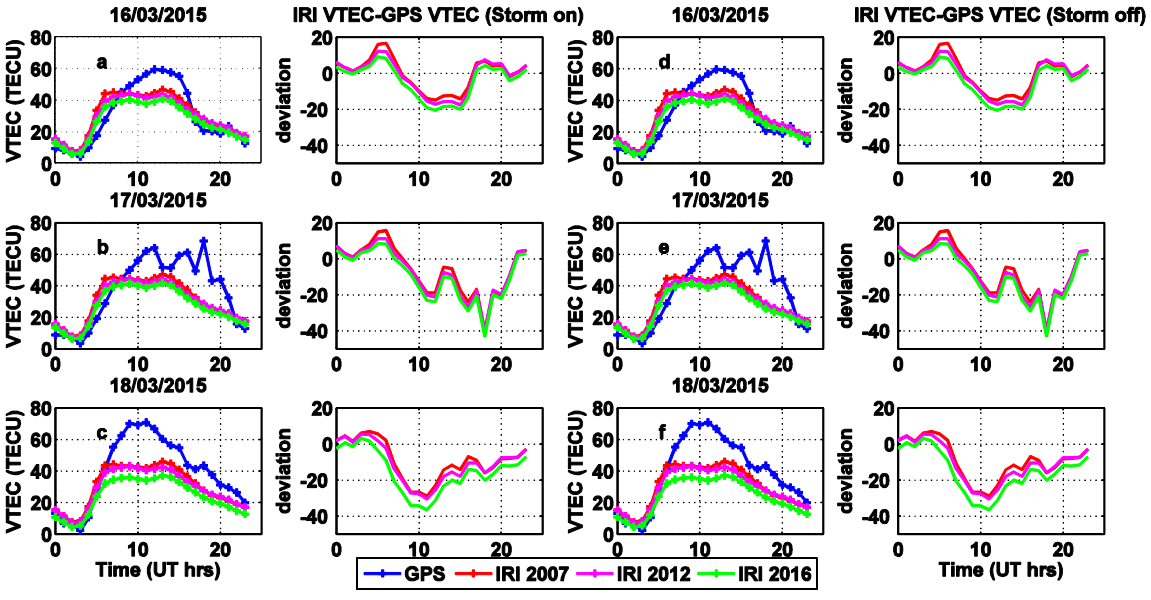

Figure 13: A graph to show the variation of the VTEC and the response of IRI model on storm time condition which occurred on March 17/2015 as observed over Arba Minch station. Figures 14a–14c and Figures 14d–14f show patterns of the modeled and measured VTEC values when the storm option is “on” and “off,” respectively.

Station	code	Geographic coordinates Lat. (N), Long. (E)	Geomagnetic coordinates Lat. (N), Long. (E)	Dip angle
Asosa	asos	(10.05,34.55)	(0.56,106.38)	3.2
Ambo	aboo	(8.97,37.86)	(0.07,109.80)	1.2
Nazret	nazr	(8.57,39.29)	(-0.08,111.27)	1.19
Arba Minch	armi	(6.06,37.56)	(-3.08,109.57)	-5.7

Table 1: Coordinates of GPS receivers used for the study